ACS Sustainable Chemistry & Engineering

pubs.acs.org/journal/ascecg

Research Article

Tuning the Solubility of the Herbicide Bentazon: from Salt to Neutral and to Inclusion Complexes

Alessandra Azzali, Simone d'Agostino,* and Fabrizia Grepioni

Cite This: *ACS Sustainable Chem. Eng.* 2021, 9, 12530–12539

Read Online

ACCESS | Metrics & More | Article Recommendations | Supporting Information

ABSTRACT: We report on the mechanochemical synthesis of inclusion complexes obtained by reacting the neutral crystalline herbicide bentazon (HBtz) with native cyclodextrins (CDs). The reaction of HBtz with γ-CD resulted in the formation of the inclusion complexes [β-CD·HBtz]·6H_2O and [γ-CD·HBtz]·8H_2O, which were characterized via a combination of X-ray diffraction, Fourier transform infrared (FTIR) spectroscopy, and calorimetric measurements. No complexation, on the contrary, was achieved upon the reaction of HBtz with α-CD. The salt NaBtz·1.75H_2O, widely used as a water-soluble salt of bentazon for the manufacturing of agrochemicals, was also synthesized and structurally characterized, and its solubility and dissolution properties were compared to those of neutral HBtz and of the β-CD and γ-CD inclusion complexes. It was found that the behavior of [β-CD·HBtz]·6H_2O and [γ-CD·HBtz]·8H_2O in water is similar, with dissolution rates of 28.4 ng·L^{-1}·min^{-1} and 39.8 ng·L^{-1}·min^{-1}, respectively, and is intermediate between those of NaBtz·1.75H_2O (228 ng·L^{-1}·min^{-1}) and neutral bentazon (3.5 ng·L^{-1}·min^{-1}). These results were also compared with those of the dehydrated inclusion complexes, which displayed intermediate dissolution rates between hydrous complexes and NaBtz·1.75H_2O. All findings indicate that the inclusion of HBtz in β-CD and γ-CD might represent a viable alternative for the preparation of environmentally friendly agrochemicals with controlled bentazon release to be used in the formulation of herbicides.

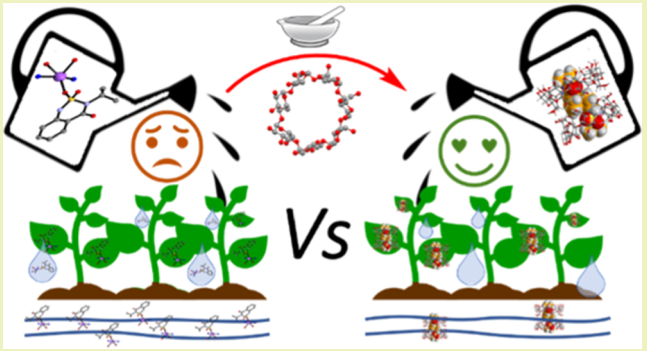

KEYWORDS: *bentazon, herbicides, native cyclodextrins, inclusion complexes, mechanochemistry*

INTRODUCTION

Bentazon (HBtz) is a cyclic sulfonamide employed as a selective, contact herbicide for postemergent weed control of broad-leaved weeds in a wide variety of cultivations.[1] Since it must be applied aerially or through contact spraying on cultivations, its scarce aqueous solubility represents the main factor that limits its utility, and the formation of its sodium salt (known as sodium bentazon) is the only method employed, so far, to address this shortcoming (Scheme 1).[2] The solubility of sodium bentazon, however, is considerably increased with respect to pure bentazon, resulting in excess contamination of water resources. The pollution of water is a topic of considerable environmental interest, owing to the increasing number of pesticides detected in waters and to the establishment of strict directives in Europe, aiming at the protection of water sources used for the production of drinking water.[3−5]

Bentazon is classified as slightly toxic (class III) by World Health Organization (WHO)[6] and noncarcinogenic to humans,[7,8] although it can undergo photodegradation in groundwater and soil.[8,9] The environmental protection agency (EPA) and the European Commission for Environmental and Human Health Risk Indicators for Agricultural Pesticides in Estuaries[10] regulated the levels of pesticide bentazon in waters and it was recently found still exceeding quality standards in groundwater, surface water, and surface water infiltration.[11] It has, in fact, low binding affinity with soil, so it can easily runoff and contribute to leaching into the ground, becoming a major concern in terms of soil and groundwater contamination.[12] Practical applications of agrochemicals are often made difficult

Scheme 1. Herbicide Bentazon (Left) and its Sodium Salt (Right)

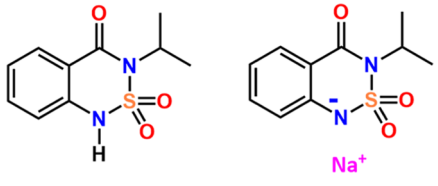

Received: April 23, 2021
Published: September 6, 2021

Scheme 2. Series of Native Cyclodextrins Used in this Work

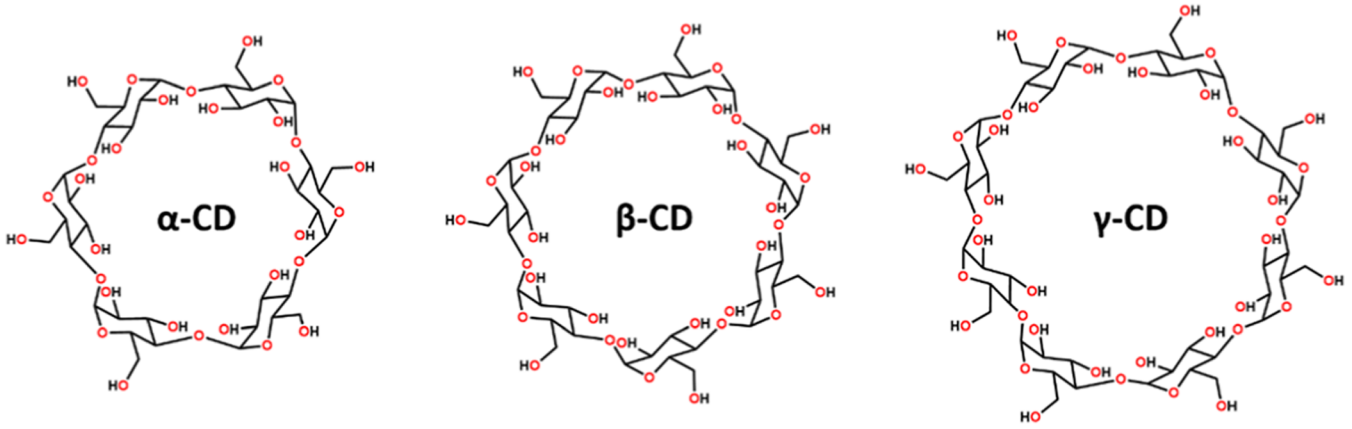

by their adverse physicochemical properties, such as poor solubility, chemical and thermal instability, toxicity to workers, malodour, volatility, high soil mobility, persistence, and poor wettability.[13] For these reasons, optimization of herbicide formulations is of paramount importance.[14−17]

A promising approach for controlling the solid-state features of molecules, in the solid state, comes from crystal engineering,[18−20] which aims to modify the solid-state properties through careful control of the interactions that lead to the assembly of components into the final solid. Within this strategy, polymorphism, cocrystallization, and salt formation are the most powerful tools used to generate a range of new bulk properties, including modulation of optical features,[21−23] enantioselectivity,[24,25] and solubility in water,[26,27] among others. For these reasons, the preparation of cocrystals and salts, as well as the screening of different crystal forms of a compound are not only an academic challenge but also an opportunity for innovation.

Complexation with cyclodextrins may be regarded as a special case of cocrystal formation, particularly useful when the active molecule cannot undergo proton exchange for salt formation, nor it possesses functional groups able to form strong intermolecular interactions, like hydrogen or halogen bonds. Cyclodextrins (CDs) are cyclic oligosaccharides produced from starch,[28−30] not from fossil resources, and are nontoxic;[31] all native cyclodextrins are accepted as food additives and "generally recognized as safe" (GRAS).[32,33] Thanks to their hydrophilic outer surface and internal hydrophobic cavities, CDs are able to host many nonpolar guest compounds[34] having a suitable size and shape to fit the cavity, thus forming inclusion complexes soluble in aqueous media. The principal advantage is that the guest is not permanently bound but is in a dynamic equilibrium with the CD host, therefore dissociation of the inclusion complex with the consequent guest release may occur in certain conditions, e.g., following a large increase in the number of water molecules in the surrounding environment.[34,35] For these reasons, encapsulation of molecules in cyclodextrins has been extensively investigated in the last decades, and stable inclusion complexes have been obtained with useful applications in many fields, ranging from drug delivery[36,37] to pesticides[13,35] and from cosmetics[13,38−43] to sunscreens.[44,45]

The aim of this research was twofold: on the one hand, we were interested in exploring the complexation ability of the whole series of native cyclodextrins toward the herbicide bentazon (HBtz) (see Scheme 2), using a variety of preparative methods, including mechanochemistry (i.e., grinding and kneading) and crystallization from solution; on the other hand, we wanted to compare the water dissolution properties of the inclusion complexes with those of neutral bentazon (HBtz) and of its sodium salt, NaBtz·1.75H_2O, which was structurally characterized in this work for the first time.

This study complements previously published accounts of CD inclusion complexes with agrochemicals and herbicides,[46−51] including the early results obtained by Yáñez et al., who first reported on the complexation ability and solubility features of inclusion complexes obtained by reacting bentazon with a series of native and modified β-cyclodextrin such as the sulfobutylether-β-CD (SBE-CD) and 2-hydroxypropyl-β-cyclodextrin (HPCD).[49,52,53] The improved solubility in water, the presence of harmless CD excipients, the possibility of achieving release control in the soil, and the "green" mechanochemical preparations could all positively impact the preparation of agrochemical products and, ultimately, prove to be beneficial to the environment.

EXPERIMENTAL SECTION

Materials. All reagents were purchased from Sigma-Aldrich and used without further purification. The reagents used were α-cyclodextrin (972.84 g/mol), β-cyclodextrin·8H_2O (1278.98 g/mol), γ-cyclodextrin·10H_2O (1477.12 g/mol), and bentazon (240.28 g/mol). Double-distilled water and reagent-grade solvents were used.

NaBtz·1.75H_2O. Overall, 120 mg (0.05 mmol) of bentazon was suspended in ca. 10 mL of water, then 1 equiv of NaOH (20 mg, 0.05 mmol) was added, and the resulting clear solution was stirred overnight at ambient conditions. The solution was then filtered to remove unreacted material and the solvent was left to evaporate in open air at RT. After 1 week, a white crystalline powder was recovered. Single crystals suitable for X-ray diffraction (XRD) were obtained by recrystallization from DMF.

[β-CD·HBtz]·6H_2O and [γ-CD·HBtz]·8H_2O. The inclusion complexes were obtained by ball-milling bentazon (50 mg, 0.21 mmol), for 60 min at 20 Hz in an agate jar, with 1 equiv of the corresponding native cyclodextrin (β-CD: 0.269 mg, 0.21 mmol; γ-CD: 0.310 mg, 0.21 mmol) in the presence of two drops of water (ca. 50 mg). Single crystals suitable for XRD were obtained via slow evaporation from a water solution obtained dissolving the kneading products at RT (ca. 25 °C). To facilitate the dissolution of the components, the magnetic stirrer was set at ca. 100 rpm; once a clear solution was obtained, the stirring was suspended, and the solution was left to evaporate. Alternatively, they can be grown by slow evaporation of a solution obtained by mixing equimolar amounts of bentazon and β-CD or γ-CD previously dissolved at RT in EtOH and

https://doi.org/10.1021/acssuschemeng.1c02749
ACS Sustainable Chem. Eng. 2021, 9, 12530−12539

water, respectively. Powders of the inclusion complex [γ-CD·HBtz]·8H_2O suitable for Pawley refinement were obtained using a slurry: 160 mg (0.06 mmol) of commercial γ-CD was dissolved in 5 mL of water at RT, and 1 equiv of solid bentazon (37 mg, 0.06 mmol) was added in small portions. The suspension was stirred for 1 week at ambient conditions, filtered under vacuum, and washed with cold water (3 × 1 mL). The pure inclusion complex was recovered as a white crystalline powder.

Single-Crystal XRD. Single-crystal data for NaBtz·1.75H_2O were collected at RT with an Oxford XCalibur S CCD diffractometer equipped with a graphite monochromator (Mo Kα radiation, λ = 0.71073 Å). Data for the inclusion complexes [β-CD·HBtz]·6H_2O and [γ-CD·HBtz]·8H_2O were collected at a low temperature (100 K) on a Bruker D8 Venture diffractometer, equipped with a PHOTON III detector, an IμS 3.0 microfocus X-ray source (Cu-Kα radiation, λ = 1.54056 Å), and a cryostat Oxford CryoStream800. The structures were solved by intrinsic phasing with SHELXT[54] and refined on F^2 by full-matrix least-squares refinement with SHELXL[55] implemented in Olex2 software.[56] All nonhydrogen atoms were refined anisotropically. H_{CH} atoms for all compounds were added in calculated positions and refined riding on their respective carbon atoms. H_{OH} atoms were either directly located or added at the calculated positions. Data collection and refinement details are given in Table S1. The position of bentazon and disordered water molecules in the structure of [γ-CD·HBtz]·8H_2O could not be unambiguously determined because of severe disorder; therefore, their contribution to the calculated structure factors was removed using the solvent mask function implemented in Olex2 software.[57] The program Mercury[58] was used for molecular graphics and analysis of intermolecular interactions. Crystal data can be obtained free of charge via www.ccdc.cam.ac.uk/conts/retrieving.html (or from the Cambridge Crystallographic Data Centre, 12 Union Road, Cambridge CB21EZ, U.K.; Fax: (+44)1223-336-033; or Email: deposit@ccdc.cam.ac.uk). CCDC numbers 2070875-2070877.

Powder XRD. For phase identification, diffractograms were recorded on a PANalytical X'Pert Pro automated diffractometer equipped with an X'Celerator detector in the Bragg−Brentano geometry, using Cu-Kα radiation (λ = 1.5418 Å) without a monochromator in a 2θ range between 3 and 40° (continuous scan mode, step size 0.0167°, counting time 19.685 s, Soller slit 0.04 rad, antiscatter slit 1/2, divergence slit 1/4, and 40 mA·40 kV). The program Mercury[58] was used for the calculation of the X-ray powder patterns on the basis of single-crystal data either retrieved from the Cambridge structural database (CSD) or collected in this work. For indexation and Pawley refinement purposes, X-ray powder diffractograms in a 2θ range of 3−60° (step size, 0.003°; time/step, 99s; 0.02 rad soller; and 40 mA·40 kV) were collected on a Panalytical X'Pert PRO automated diffractometer operated in a transmission mode (capillary spinner) and equipped with a Pixel detector. Powder diffraction data were analyzed using software X'pert HiScorePlus,[59] which is designed to analyze monochromatic and nonmonochromatic data. Peaks were automatically chosen in a 2θ range 4−40°, and a tetragonal cell, with the unit-cell axis very close to those determined via SCXRD (see Table S1), was found using the algorithm DICVOL04.[60] Unit-cell parameters were then refined by the Pawley method with software TOPAS4.1.[61] A shifted Chebyshev function with eight parameters was used to describe the background. Refinement converged with R_{wp} = 2.7%, χ^2 = 3.1, and R_{exp} = 0.9%. Figure S4 shows experimental, calculated, and difference curves.

IR Spectroscopy. Attenuated total reflectance Fourier transform IR (ATR-FTIR) spectra were obtained using a Bruker α FTIR spectrometer. For the inclusion complexes, ATR-FTIR spectra were run on polycrystalline samples obtained via grinding, slurry, and solution, while for all of the reactants, measurements were run on the commercially available products.

Thermogravimetric Analysis. TGA measurements on all samples were performed with a Perkin-Elmer TGA7 thermogravimetric analyzer, in a 30−400 °C temperature range, under a N_2 gas flow and at a heating rate of 5.00 °C min^{-1}.

Differential Scanning Calorimetry (DSC). DSC traces were recorded using a Perkin-Elmer Diamond differential scanning calorimeter. All samples (ca. 10 mg) were placed in open Al pans. All measurements were conducted under a N_2 atmosphere in a 30−200 °C temperature range, at a heating rate of 5.00 °C min^{-1}.

^{1}H-NMR Spectroscopy. ^{1}H-NMR spectra were recorded on a Varian INOVA 400 (400 MHz) spectrometer; the solvent used was dimethylsulfoxyde-d_6 (DMSO-d_6), bought from Sigma-Aldrich. Chemical shifts are reported in ppm, with tetramethylsilane as an internal reference standard.

UV−Vis Spectroscopy. UV−vis spectra were recorded in a water solution with an Agilent Cary 60 UV−vis spectrophotometer.

Dissolution Rate Measurements. Dissolution rate measurements were performed at 295 K at a stirring rate of 100 rpm. [β-CD·HBtz]·6H_2O, [γ-CD·HBtz]·8H_2O, bentazon, and NaBtz·1.75H_2O (8−10 mg of the inclusion complexes, corresponding on average to 1.7 mg of bentazon, 3 mg of bentazon, and 5 mg of its sodium salt, corresponding to 3.6 mg of bentazon) were added to 70 mL of deionized water, and measurements were carried out to reach a plateau (20 min for all, except for 35 min for [β-CD·HBtz]·6H_2O and 80 min for bentazon) using a Varian Cary 50 spectrophotometer equipped with an optic-fiber dip probe. The wavelengths used to follow the dissolutions are the same as those reported for calibration curves (see SI). In the case of the anhydrous compounds, each sample was kept at 60 °C for 72 h and measured immediately afterward. The resulting values for all measurements were then converted from absorbance to concentration, via the calibration curves reported in Figures S18−S21.

Solubility Measurements. Solubility was measured by stirring saturated water solutions of [β-CD·HBtz]·6H_2O and [γ-CD·HBtz]·8H_2O for 24 h. After stirring, they were centrifuged at 5000 rpm for 30 min, and then the solutions were filtered with a 0.45 μm syringe filter. Overall, 250 μL was collected from each solution and added to previously weighed vials. After evaporation, the vials were weighed again. The resulting values were averaged on five samples for each compound.

Optical Microscopy. Images of single-crystal specimens of [β-CD·HBtz]·6H_2O and [γ-CD·HBtz]·8H_2O were taken under polarized light using an OLYMPUS BX41 microscope equipped with a NIKON DS FI3 camera, and are shown in Figure S24.

RESULTS AND DISCUSSION

Inclusion Complexes and Bentazon Sodium Salt: Synthesis and Solid-State Characterization. We have focused our attention mainly on preparing the inclusion complexes via mechanochemistry, viz. grinding and kneading. To this end, solid bentazon (HBtz) and native cyclodextrins (α-CD, β-CD, and γ-CD) were ground together with and without a catalytic amount of water; the products were then analyzed with powder XRD and FTIR spectroscopy to assess complexation between CDs and HBtz in the solid state. Monitoring the position of the C═O stretching band represents a good indicator for the formation of inclusion complexes, as the C═O stretching mode is quite sensitive to weak intermolecular interactions,[38] and the hydrophobic cavity of the cyclodextrins affects the relative contributions of the nonpolarized and polarized resonance structures of the C═O bond (C═O and $^+$C−O$^-$, respectively), as also observed for other inclusion complexes.[38,49,62−65]

As shown in Figure 1, the band for the C═O stretching occurs at 1645 cm^{-1} in the spectrum of pure HBtz, whereas a new and blue-shifted band appears at 1689 and 1687 cm^{-1} in the spectra of the products obtained via kneading with β-CD and γ-CD, respectively. These results are also in good agreement with previously IR data presented from Yáñez et al.[49,52] According to the literature,[49,63,66] these blue shifts arise from the stabilization of the nonpolarized resonance structure

https://doi.org/10.1021/acssuschemeng.1c02749
ACS Sustainable Chem. Eng. 2021, 9, 12530−12539

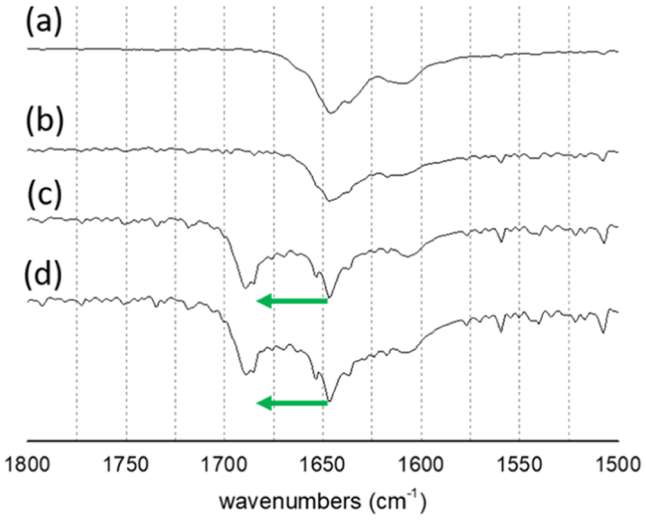

Figure 1. Comparison of the FTIR spectra recorded for pure bentazon (a) and on the solids obtained by kneading HBtz with α-CD (b), β-CD (c), and γ-CD (d).

of the C═O bond, as well as from the disruption of the hydrogen bonding interaction between molecules of pure HBtz (N−H···O═C), thus giving a first indication of the presence of a monomeric bentazon in the cyclodextrin cavity. Inclusion of bentazon in α-CD, on the contrary, was not successful, as no shift was detected for the C═O band in the products obtained either via grinding or kneading (see Figure 1b). Comparisons between the IR spectra of the components, bentazon and CDs, and the products obtained via grinding and kneading are shown in Figures S5−S7.

Figure 2 shows a comparison between the experimental X-ray powder patterns for the starting materials (HBtz and the three cyclodextrins) and, as an example, the pattern for the LAG product of γ-CD and HBtz, as well as the ones obtained via a solution and a slurry. In the absence of water, the grinding process resulted in a physical mixture of the reagents, whereas the addition of a few drops of water yielded a new crystalline

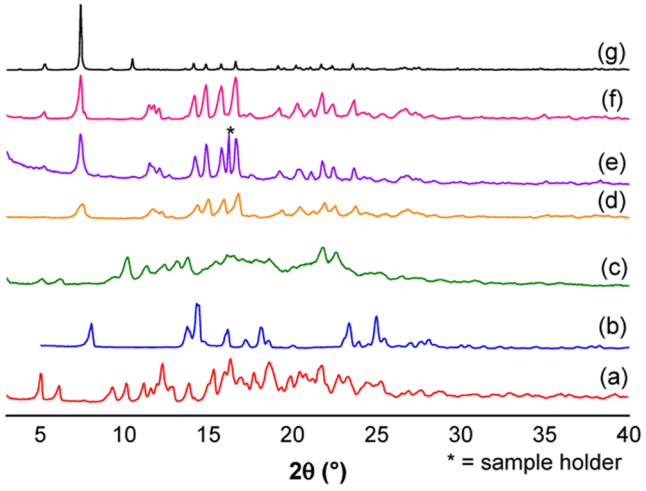

Figure 2. Comparison of the experimental powder XRD patterns for: (a) γ-CD, (b) HBtz (form I), (c) grinding product, (d) kneading product, (e) solution product, (f) slurry product, and (g) calculated reference pattern for the refcode SIBJAO, chosen as representative of the tetragonal $P42_12$ isostructural series.[69]

phase, perfectly superimposable to the ones obtained from the solution and the slurry. It is worth noting how they all closely resemble the reference pattern for the tetragonal $P42_12$ isostructural series for γ-CD inclusion complexes.[38,48,67,68] Analogous behavior was observed for the synthesis of the inclusion complex with β-CD; in this case, the X-ray pattern for the product is similar to those of the isostructural series $P1$ or $C2$, corresponding to channel-type structures of β-CD complexes.[38,48,67,68] In the case of α-CD, on the other side, both the grinding and kneading processes with HBtz resulted in a physical mixture of the starting compounds.

These findings suggest that the cavities of β-CD and γ-CD, with a free volume of 262 Å^3 and 427 Å^3,[35] respectively, are more effective in hosting molecular bentazon (with a molecular volume of ca. 260 Å^3), while the cavity in α-CD, with a volume of 174 Å^3,[35] is too small to host the herbicide molecule. The mechanochemical synthesis was repeated with an α-CD:HBtz stoichiometric ratio of 2:1, in the attempt to force an encapsulation for bentazon by two α-CD molecules; also in this case, however, no evidence of inclusion complex formation was detected.

Single crystals for the kneading products of HBtz with β-CD and γ-CD were grown from solution; even after many attempts, only a tiny and poorly diffracting specimen could be obtained, but a detailed structural characterization was still possible, especially in the case of the β-CD inclusion complex.

The inclusion complex [β-CD·HBtz]·6H_2O crystallizes in the triclinic space group $P1$ with two β-cyclodextrins in the asymmetric unit, each β-CD including a molecule of bentazon in the hydrophobic cavity. Six water molecules per formula unit could also be detected. The β-CD molecules are stacked in pairs, slightly tilted with respect to each other, along the crystallographic b-axis (see Figure 3), thus forming the channel-type structure typically observed for β-CD inclusion compounds in the $P1$ isostructural series;[67,68,70−72] hydrogen bonds connect the β-CD molecules via the glucopyranose units [$O_{OH}\cdots O_{OH}$ = 2.721(1) − 2.973(9) Å]. HBtz molecules are arranged "head-to-tail" within a dimeric β-CD pair (see Figure 3c) in such a way as to maximize the $\pi-\pi$ interaction between the aromatic rings [d = 3.452(1) Å]; hydrogen bonds are also present inside the cavities between the NH group on HBtz and the glycosidic O atoms on β-CD [$N_{NH}\cdots O_g$ = 2.99(1), 2.95(1) Å].

Crystalline [γ-CD-Hbtz]·8H_2O represents a more difficult case, and we were unable to fully modeling the structure because of the disorder affecting the bentazon molecule inside the hydrophobic cavity. The host γ-CD molecules lie on a fourfold symmetry rotational axis and display the expected channel-like structure typical of the tetragonal $P42_12$ isostructural series for γ-CD inclusion complexes (see Figure 4).[67,68,70] The channels run parallel to the crystallographic c-axis, and the γ-CD molecules interact along the channel via hydrogen bonds between the glucopyranose units [$O_{OH}\cdots O_{OH}$ = 2.815(3) − 2.998(4) Å] (see Figure 4a).

The water molecules present in the crystal occupy the cavities between the channels, forming hydrogen bonds with the host molecules. Due to the large size of the γ-CD hydrophobic cavity, the bentazon molecule is free to occupy different orientations with respect to the rotational axis; for this reason, it was not possible to locate with confidence the position of the bentazon atoms; the same problem was encountered with the water molecules outside the cavity. The contribution of HBtz and H_2O molecules was therefore

https://doi.org/10.1021/acssuschemeng.1c02749
ACS Sustainable Chem. Eng. 2021, 9, 12530−12539

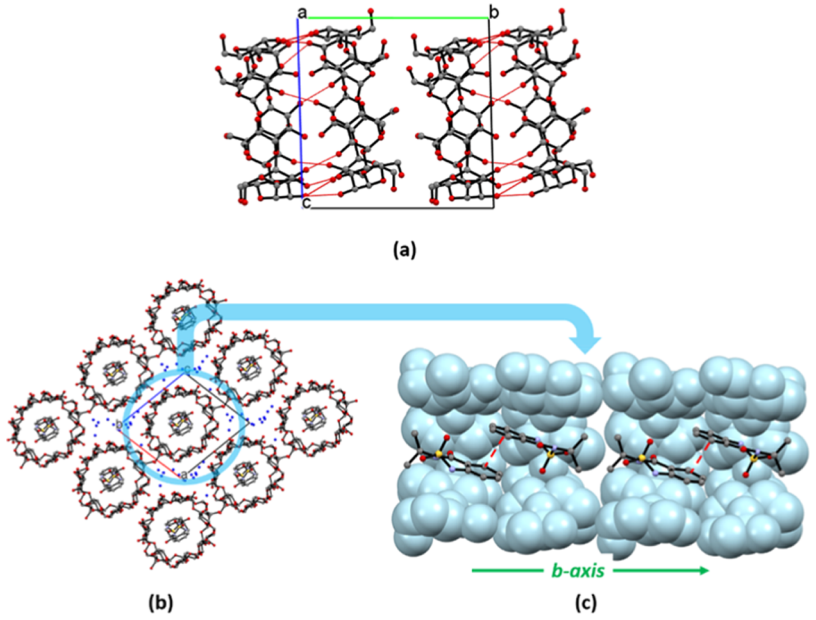

Figure 3. Relevant packing features in crystalline [β-CD·HBtz]·6H_2O: (a) Stacking of the β-CD molecules along the crystallographic *b*-axis in crystalline, showing the channel-like structure typical of the *P*1 isostructural series; (b) projection down the *b*-axis showing the channel-like structure hosting the HBtz molecules, with water molecules (in blue) filling the cavities outside the channels; and (c) section of one channel, with walls (β-CD molecules) in light blue, showing the $\pi-\pi$ interaction between the aromatic rings of the guest molecules. H atoms are omitted for clarity.

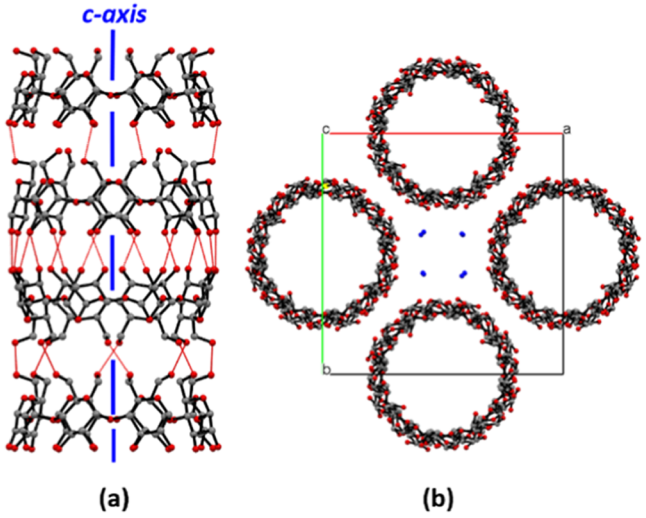

Figure 4. (a) Channel-like structure formed by the host molecule in crystalline [γ-CD·HBtz]·8H_2O and (b) crystal packing viewed along the *c*-axis. H atoms are omitted for clarity, and water molecules are shown in blue.

subtracted in the refinement procedure (see the Experimental Section). The heavy disorder inside the cavity of γ-CD is supported by the fact that: (i) the guest molecules are located within infinite channels of the C_4 symmetry, typical of the tetragonal $P42_12$ isostructural series, generated by overlapping the central cavities of the stacked γ-CD molecules;[68] (ii) only guests also possessing a fourfold symmetry are usually located well inside the channel;[73] and (iii) the volume of the γ-CD cavity is large enough to allow for the orientational disorder of HBtz around the molecular main axis (see Figure 5). The possibility that the inclusion complex might have formed with a substoichiometric amount of guest, i.e., with an HBtz/γ-CD ratio <1, was ruled out, as ^{1}H-NMR solution spectra for a polycrystalline sample were obtained via a slurry, which showed the same unit cell determined via SCXRD (see Pawley refinement in Figure S4), confirming a 1:1 stoichiometric ratio (see Figure S8).

Finally, we shall also discuss in short, the main structural features, obtained via single-crystal X-ray diffraction, of the sodium bentazon salt. The salt NaBtz·1.75H_2O crystallizes in the triclinic $P\bar{1}$ space group, with four ionic pairs and seven water molecules in the asymmetric unit.

The geometry and the intramolecular distances/angles for all four independent molecules are almost coincident with those observed for HBtz form I (CSD refcode FAXWAB); it is difficult, judging from a comparison of these data, to assign the negative charge to the nitrogen or the carbonyl oxygen, i.e., to define the anion as the result of the deprotonation of the keto or enol form of neutral bentazon (Scheme 3); in the solid state, the charge is probably delocalized (short distances to the sodium cation are observed both for the oxygen and nitrogen atoms [Na···$O_{S=O}$ = 2.299(5) − 2.482(7) Å, Na···O_W = 2.25(1) − 2.691(8) Å, and Na···$O_{C=O/C-O}$ − = 2.313(6) − 2.360(6) Å]) although a short value of the C−O distance in all anions seems to hint at the presence of a C=O double bond.

Bentazon anions in crystalline NaBtz·1.75H_2O are arranged in such a way as to form channels extending parallel to the crystallographic [101] direction (see Figure 6a); the channels are filled with the sodium cations and the water molecules (Figure 6b).

Thermal Behavior of the Inclusion Complexes. Crystalline bentazon is stable up to ca. 140 °C (Figure S10, bottom), while TGA traces for hydrated β-CD and γ-CD show first a weight loss, corresponding to dehydration, in the 40−100 °C range, followed by complete degradation starting at ca. 280 °C. TGA traces for the β-CD and γ-CD inclusion complexes are characterized by a weight loss, complete at ca. 100 °C, corresponding to ca. six and eight water molecules, respectively, thus defining the inclusion complexes formulae as

https://doi.org/10.1021/acssuschemeng.1c02749
ACS Sustainable Chem. Eng. 2021, 9, 12530−12539

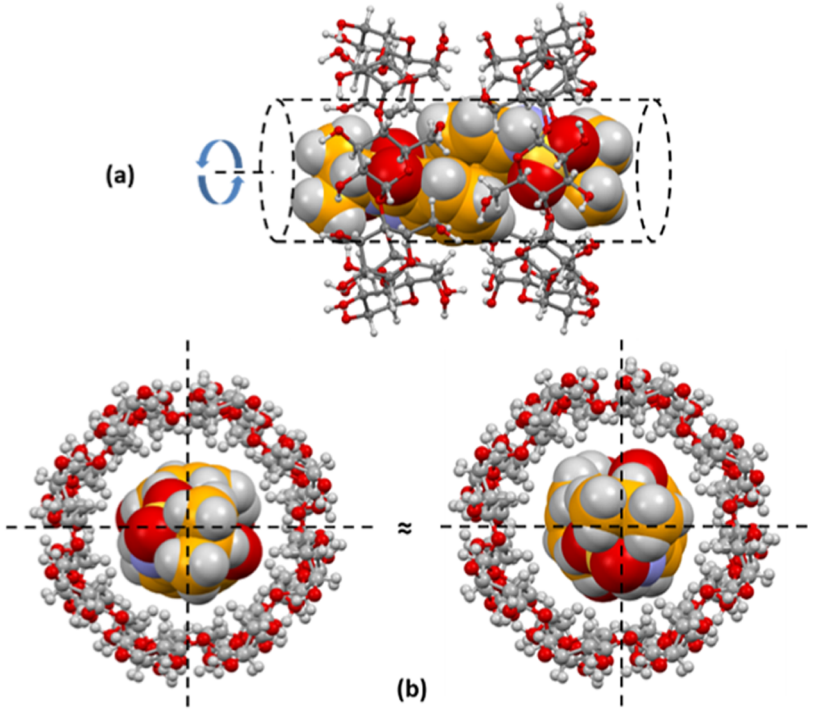

Figure 5. Depiction of disorder for bentazon within the γ-CD host likely to occur in crystalline [γ-CD·HBtz]·8H_2O. The two molecules of HBtz, interacting via π stacking inside the large cavities of the γ-CD dimeric unit, have the shape of a cylinder (a), and this can assume different orientations around the channel axis: two possible orientations are graphically presented here (b).

Scheme 3. Keto−Enol Tautomerism Observed for Neutral Bentazon in Solution.[74,75]

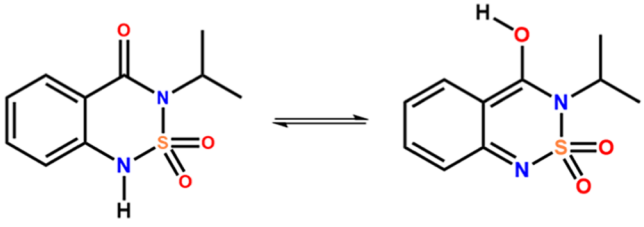

[β-CD·HBtz]·6H_2O and [γ-CD·HBtz]·8H_2O. It is interesting to note that decomposition of the inclusion compounds starts only at ca. 180−200 °C: the thermal stability of bentazon is thus enhanced, and its degradation accompanies that of the β- and γ-cyclodextrins.

DSC traces for pure β-CD and γ-CD show a broad endothermic peak centered at ca. 114 and 87 °C (Figure S10), respectively, which can be attributed to dehydration processes; dehydration can also be observed for the inclusion compounds (see Figures S11 and S14). DSC measurement for pure HBtz shows an endothermic peak corresponding to melting at 140 °C;[76] the peak is still present in the physical mixtures resulting from the grinding processes with β-CD and γ-CD (see Figures S13 and S16), but it is absent in the DSC traces of the inclusion compounds, obtained via kneading. These results are consistent with the results of FTIR spectroscopy and X-ray diffraction analyses.

Dissolution Studies. Dissolution rates were measured for and compared between polycrystalline samples of pure HBtz, NaBtz·1.75H_2O, [β-CD·HBtz]·6H_2O, [γ-CD·HBtz]·8H_2O, and the dehydration products of the inclusion complexes.

As evidenced in Figure 7, a clear trend can be observed among the series of compounds: pure bentazon shows the lowest dissolution rate (0.0147 mmol·L^{-1}·min^{-1} or 3.5 ng·L^{-1}·min^{-1}), while the sodium salt, NaBtz·1.75H_2O, showed the highest dissolution rate, 0.335 mmol·L^{-1}·min^{-1} (228 ng·L^{-1}·min^{-1}).

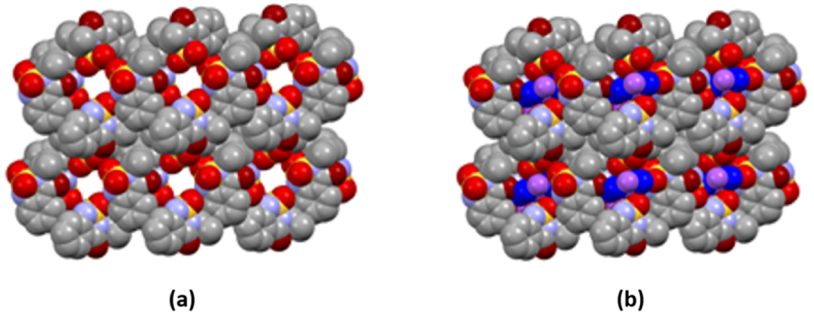

Figure 6. Channels in crystalline NaBtz·1.75H_2O, formed by the bentazon anions (a) and the channels are filled with sodium cations (in violet) and water molecules (in blue) (b). H atoms are omitted for clarity.

https://doi.org/10.1021/acssuschemeng.1c02749
ACS Sustainable Chem. Eng. 2021, 9, 12530−12539

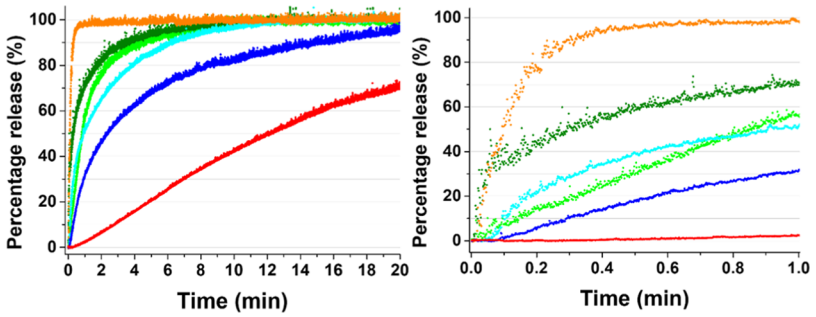

Figure 7. Dissolution rate graphs in percentage release normalized on plateau values and magnification. Color scheme: Bentazon (red), [β-CD·HBtz]·6H_2O (blue), anhydrous [β-CD·HBtz] (light blue), [γ-CD·HBtz]·8H_2O (light green), anhydrous [γ-CD·HBtz] (green), and NaBtz·1.75H_2O (orange). Dissolution rate graphs in mmol·L^{-1}·min^{-1} and in ng·L^{-1}·min^{-1} can be found in Figures S22 and S23.

The hydrated inclusion complexes obtained with β-CD and γ-CD dissolve with rates of 0.021 mmol·L^{-1}·min^{-1} (28.4 ng·L^{-1}·min^{-1}) and 0.0259 mmol·L^{-1}·min^{-1} (39.8 ng·L^{-1}·min^{-1}) for [β-CD·HBtz]·6H_2O and [γ-CD·HBtz]·8H_2O, respectively. Dissolution rates were measured also on dehydrated inclusion complexes [β-CD·HBtz] and [γ-CD·HBtz] (see Figures S9, S12, and S15 for characterization) and their values are 0.0251 mg·L^{-1}·min^{-1} (33.2 ng·L^{-1}·min^{-1}) and 0.133 mmol L^{-1} min^{-1} (205 ng·L^{-1}·min^{-1}), respectively. As expected, as this is usually the case when comparing anhydrous and hydrated compounds, dissolution in water is faster for [β-CD·HBtz] and [γ-CD·HBtz] with respect to [β-CD·HBtz]·6H_2O and [γ-CD·HBtz]·8H_2O. The dissolution rates for the anhydrous forms, however, are still lower than the one determined for NaBtz·1.75H_2O; for [β-CD·HBtz]·6H_2O, the difference is of one order of magnitude.

Solubility in water was also measured for all compounds, and the values are given in Table 1. With respect to pure bentazon, the solubility of [β-CD·HBtz]·6H_2O shows a higher value, and this is even more pronounced in the case of [γ-CD·HBtz]·8H_2O. According to our dissolution rate study, for both compounds, the solubility is lower compared to that for NaBtz·1.75H_2O, which is the solid form currently commercialized and used in the fields. Inclusion of bentazon in cyclodextrins would, therefore, make spray loading of this herbicide, previously dissolved in water, a viable process. At the same time, the lower solubility, compared to that of NaBtz·1.75H_2O, would help in preventing its leaching into ground water.

Table 1. Summary of the Solubilities of the Studied Compounds, Expressed in mg mL^{-1}

compound	mg mL^{-1}
bentazon	0.49[9,77−80]
NaHBtz·1.75H_2O	230[77,78,81]
[β-CD·HBtz]	1.17
[γ-CD·HBtz]	1.80
[β-CD·HBtz]·6H_2O	1.26
[γ-CD·HBtz]·8H_2O	1.97

CONCLUSIONS

In this work, we reported on the synthesis and structural characterization of two new inclusion complexes obtained by reacting the native cyclodextrins β-CD and γ-CD with the herbicide bentazon, viz. [β-CD·HBtz]·6H_2O, and [γ-CD·HBtz]·8H_2O. The novel compounds were assembled in a solid state via mechanochemistry (kneading with water), exploiting the cyclodextrins hydrophobic effect. Additionally, the salt NaBtz·1.75H_2O, commonly used to make HBtz soluble in water and for the manufacturing of commercial pesticides, was also synthesized and structurally characterized.

Dissolution rates and solubilities in water were measured for all compounds, and a clear trend was observed. The increase is definitely larger for the sodium salt, whereas for the inclusion complexes, [β-CD·HBtz]·6H_2O and [γ-CD·HBtz]·8H_2O, it is intermediate. The anhydrous counterparts, [β-CD·HBtz] and [γ-CD·HBtz], provided an additional "fine" tuning of the dissolution rates.

This study proves that the inclusion of nonsoluble molecules in cyclodextrins would represent a viable route to overcome the solubility issues of a widely employed herbicide and to allow for spray loading processes. At the same time, the lower dissolution rate and solubility, compared to those of the sodium bentazon salt, suggest that complexation could help in preventing the herbicide to leach into ground water. Cost issues might be relevant in selecting one of the two host−guest systems: as β-CD is cheaper than its larger homologue γ-CD, [β-CD·HBtz]·6H_2O could be more suitable for scale-up production.

Work is in progress to further extend this strategy to other molecules of agrochemical, cosmetic, and pharmaceutical interests.

ASSOCIATED CONTENT

Supporting Information

The Supporting Information is available free of charge at https://pubs.acs.org/doi/10.1021/acssuschemeng.1c02749.

Crystallographic details, PXRD patterns, Pawley refinement plots, FTIR and ^{1}H-NMR spectra, TGA measurements, DSC traces, and X-ray crystallographic data for (β-CD·HBtz)·6H_2O, (γ-CD·HBtz)·8H_2O, and NaBtz·1.75H_2O (PDF)

AUTHOR INFORMATION

Corresponding Author

Simone d'Agostino − *Dipartimento di Chimica "Giacomo Ciamician", Università di Bologna, 40126 Bologna, Italy;* orcid.org/0000-0003-3065-5860; Email: simone.dagostino2@unibo.it

Authors

Alessandra Azzali − *Dipartimento di Chimica "Giacomo Ciamician", Università di Bologna, 40126 Bologna, Italy*

Fabrizia Grepioni − *Dipartimento di Chimica "Giacomo Ciamician", Università di Bologna, 40126 Bologna, Italy;* orcid.org/0000-0003-3895-0979

Complete contact information is available at: https://pubs.acs.org/10.1021/acssuschemeng.1c02749

Author Contributions

This manuscript was written through the contributions of all authors. All authors have given approval to the final version of the manuscript.

Notes

The authors declare no competing financial interest.

■ ACKNOWLEDGMENTS

The authors acknowledge the University of Bologna (RFO-2019). They also thank Dr. Stefano Grilli for his help with NMR measurements.

■ REFERENCES

(1) Spaltro, A.; Simonetti, S.; Laurella, S.; Ruiz, D.; Compañy, A. D.; Juan, A.; Allegretti, P. Adsorption of Bentazone and Imazapyc from Water by Using Functionalized Silica: Experimental and Computational Analysis. *J. Contam. Hydrol.* **2019**, *227*, No. 103542.

(2) Pesticide Info. Bentazon salt. https://www.pesticideinfo.org/chemical/PRI1552 (accessed Mar 29, 2021).

(3) Rahemi, V.; Garrido, J. M. P. J.; Borges, F.; Brett, C. M. A.; Garrido, E. M. P. J. Electrochemical Determination of the Herbicide Bentazone Using a Carbon Nanotube β-Cyclodextrin Modified Electrode. *Electroanalysis* **2013**, *25*, 2360−2366.

(4) Hamilton, D. J.; Ambrus, Á.; Dieterle, R. M.; Felsot, A. S.; Harris, C. A. Regulatory Limits for Pesticide Residues in Water. *Chem. Int. – Newsmag. IUPAC* **2003**, *25*, 1123−1155.

(5) Directive 2000/60/EC of the European Parliament and of the Council of 23 October 2000 establishing a framework for Community action in the field of water policy. https://eur-lex.europa.eu/legal-content/EN/TXT/?uri=celex:32000L0060 (accessed Mar 29, 2021).

(6) The WHO Recommended Classification of Pesticides by Hazard. 2021, https://www.who.int/ipcs/publications/pesticides_hazard_rev_3.pdf (accessed Mar 29, 2021).

(7) U.S. Environmental Protection Agency. Toxicologicalreview of Bentazon. https://iris.epa.gov/static/pdfs/0134tr.pdf (accessed Mar 29, 2021).

(8) EXTOXNET Extension Toxicology Network Pesticide Information Profiles. Bentazon. http://extoxnet.orst.edu/pips/bentazon.htm (accessed Mar 29, 2021).

(9) Wauchope, R. D.; Buttler, T. M.; Hornsby, A. G.; Augustijn-Beckers, P. W. M.; Burt, J. P. The SCS/ARS/CES Pesticide Properties Database for Environmental Decision-Making. In *Reviews of Environmental Contamination and Toxicology: Continuation of Residue Reviews*; Ware, G. W., Ed.; Springer: New York, NY, 1992; pp 1−155.

(10) U.S. Environmental Protection Agency. R.E.D.FACTS Bentazon. https://archive.epa.gov/pesticides/reregistration/web/pdf/0182fact.pdf.

(11) Swartjes, F. A.; Van der Aa, M. Measures to Reduce Pesticides Leaching into Groundwater-Based Drinking Water Resources: An Appeal to National and Local Governments, Water Boards and Farmers. *Sci. Total Environ.* **2020**, *699*, 134186−134197.

(12) Huber, R.; Otto, S. Environmental Behavior of Bentazon Herbicide. *Reviews of Environmental Contamination and Toxicology*; Springer: New York, NY, 1994.

(13) Dodziuk, H.; Hashimoto, H.; Morillo, E.; Bilewicz, R.; Chmurski, K. Applications Other Than in the Pharmaceutical Industry *Cyclodextrins and Their Complexes*; John Wiley & Sons, Ltd, 2006; 450−473.

(14) Knowles, A. Recent Developments of Safer Formulations of Agrochemicals. *Environmentalist* **2008**, *28*, 35−44.

(15) Yusoff, S. N. M.; Kamari, A.; Aljafree, N. F. A. A Review of Materials Used as Carrier Agents in Pesticide Formulations. *Int. J. Environ. Sci. Technol.* **2016**, *13*, 2977−2994.

(16) Nir, S.; Undabeytia, T.; Yaron-Marcovich, D.; El-Nahhal, Y.; Polubesova, T.; Serban, C.; Rytwo, G.; Lagaly, G.; Rubin, B. Optimization of Adsorption of Hydrophobic Herbicides on Montmorillonite Preadsorbed by Monovalent Organic Cations: Interaction between Phenyl Rings. *Environ. Sci. Technol.* **2000**, *34*, 1269−1274.

(17) Tominack, R. L.; Tominack, R. Herbicide Formulations. *J. Toxicol. Clin. Toxicol.* **2000**, *38*, 129−135.

(18) Desiraju, G. R. Crystal Engineering: From Molecule to Crystal. *J. Am. Chem. Soc.* **2013**, *135*, 9952−9967.

(19) Braga, D.; Grepioni, F.; Maini, L.; d'Agostino, S. From Solid-State Structure and Dynamics to Crystal Engineering. *Eur. J. Inorg. Chem.* **2018**, *2018*, 3597−3605.

(20) Braga, D.; Grepioni, F.; Maini, L.; D'Agostino, S. Making Crystals with a Purpose; A Journey in Crystal Engineering at the University of Bologna. *IUCrJ* **2017**, *4*, 369−379.

(21) Yu, P.; Zhen, Y.; Dong, H.; Hu, W. Crystal Engineering of Organic Optoelectronic Materials. *Chem* **2019**, *5*, 2814−2853.

(22) Christopherson, J. C.; Topić, F.; Barrett, C. J.; Friščić, T. Halogen-Bonded Cocrystals as Optical Materials: Next-Generation Control over Light-Matter Interactions. *Cryst. Growth Des.* **2018**, *18*, 1245−1259.

(23) D'Agostino, S.; Grepioni, F.; Braga, D.; Moreschi, D.; Fattori, V.; Delchiaro, F.; Di Motta, S.; Negri, F. Exciton Coupling in Molecular Salts of 2-(1,8-Naphthalimido)Ethanoic Acid and Cyclic Amines: Modulation of the Solid-State Luminescence. *CrystEngComm* **2013**, *15*, 10470−10480.

(24) Rekis, T.; Bērziņš, A.; Orola, L.; Holczbauer, T.; Actiņš, A.; Seidel-Morgenstern, A.; Lorenz, H. Single Enantiomer's Urge to Crystallize in Centrosymmetric Space Groups: Solid Solutions of Phenylpiracetam. *Cryst. Growth Des.* **2017**, *17*, 1411−1418.

(25) Rekis, T.; D'Agostino, S.; Braga, D.; Grepioni, F. Designing Solid Solutions of Enantiomers: Lack of Enantioselectivity of Chiral Naphthalimide Derivatives in the Solid State. *Cryst. Growth Des.* **2017**, *17*, 6477−6485.

(26) Fandaruff, C.; Chelazzi, L.; Braga, D.; Cuffini, S. L.; Silva, M. A. S.; Resende, J. A. L. C.; Dichiarante, E.; Grepioni, F. Isomorphous Salts of Anti-HIV Saquinavir Mesylate: Exploring the Effect of Anion-Exchange on Its Solid-State and Dissolution Properties. *Cryst. Growth Des.* **2015**, *15*, 5233−5239.

(27) Almarsson, Ö.; Zaworotko, M. J. Crystal Engineering of the Composition of Pharmaceutical Phases. Do Pharmaceutical Co-Crystals Represent a New Path to Improved Medicines? *Chem. Commun.* **2004**, *17*, 1889−1896.

(28) Koo, Y. S.; Ko, D. S.; Jeong, D. W.; Shim, J. H. Development and Application of Cyclodextrin Hydrolyzing Mutant Enzyme Which Hydrolyzes β- and γ-CD Selectively. *J. Agric. Food Chem.* **2017**, *65*, 2331−2336.

(29) Terada, Y.; Yanase, M.; Takata, H.; Takaha, T.; Okada, S. Cyclodextrins Are Not the Major Cyclic α-1,4-Glucans Produced by the Initial Action of Cyclodextrin Glucanotransferase on Amylose. *J. Biol. Chem.* **1997**, *272*, 15729−15733.

(30) Terada, Y.; Sanbe, H.; Takaha, T.; Kitahata, S.; Koizumi, K.; Okada, S. Comparative Study of the Cyclization Reactions of Three Bacterial Cyclomaltodextrin Glucanotransferases. *Appl. Environ. Microbiol.* **2001**, *67*, 1453−1460.

(31) Waalkens-Berendsen, D. H.; Smits-Van Prooije, A. E.; Bär, A. Embryotoxicity and Teratogenicity Study with α-Cyclodextrin in Rabbits. *Regul. Toxicol. Pharmacol.* **2004**, *39*, 40−46.

(32) European Medicine agency. Cyclodextrins used as Excipients. https://www.ema.europa.eu/en/documents/scientific-guideline/questions-answers-cyclodextrins-used-excipients-medicinal-products-human-use_en.pdf (accessed Mar 29, 2021).

(33) Food and Drug Administration. GRAS NOTICE FOR ALPHA-CYCLODEXTRIN. https://www.fda.gov/media/101653/download (accessed Mar 29, 2021).

(34) Harata, K. Crystallographic Study of Cyclodextrins and Their Inclusion Complexes. *Cyclodextrins and Their Complexes*; John Wiley & Sons, Ltd, 2006; pp 147−198.
(35) Del Valle, E. M. M. Cyclodextrins and Their Uses: A Review. *Process Biochem.* **2004**, *39*, 1033−1046.
(36) Haimhoffer, Á.; Rusznyák, Á.; Réti-Nagy, K.; Vasvári, G.; Váradi, J.; Vecsernyés, M.; Bácskay, I.; Fehér, P.; Ujhelyi, Z.; Fenyvesi, F. Cyclodextrins in Drug Delivery Systems and Their Effects on Biological Barriers. *Sci. Pharm.* **2019**, *87*, 33−54.
(37) Uekama, K.; Hirayama, F.; Arima, H. Pharmaceutical Applications of Cyclodextrins and Their Derivatives. *Cyclodextrins and Their Complexes*; John Wiley & Sons, Ltd, 2006; pp 381−422.
(38) Ramos, A. I.; Braga, T. M.; Silva, P.; Fernandes, J. A.; Ribeiro-Claro, P.; De Fátima Silva Lopes, M.; Paz, F. A. A.; Braga, S. S. Chloramphenicol·cyclodextrin Inclusion Compounds: Co-Dissolution and Mechanochemical Preparations and Antibacterial Action. *CrystEngComm* **2013**, *15*, 2822−2834.
(39) Davis, M. E.; Brewster, M. E. Cyclodextrin-Based Pharmaceutics: Past, Present and Future. *Nat. Rev. Drug Discov.* **2004**, *3*, 1023−1035.
(40) Kurkov, S. V.; Loftsson, T. Cyclodextrins. *Int. J. Pharm.* **2013**, *453*, 167−180.
(41) Braga, S. S. Cyclodextrins: Emerging Medicines of the New Millennium. *Biomolecules* **2019**, *9*, 801.
(42) Hedges, A. R. Industrial Applications of Cyclodextrins. *Chem. Rev.* **1998**, *98*, 2035−2044.
(43) Loftsson, T.; Brewster, M. E. Pharmaceutical Applications of Cyclodextrins. 1. Drug Solubilization and Stabilization. *J. Pharm. Sci.* **1996**, *85*, 1017−1025.
(44) D'Agostino, S.; Azzali, A.; Casali, L.; Taddei, P.; Grepioni, F. Environmentally Friendly Sunscreens: Mechanochemical Synthesis and Characterization of β-CD Inclusion Complexes of Avobenzone and Octinoxate with Improved Photostability. *ACS Sustainable Chem. Eng.* **2020**, *8*, 13215−13225.
(45) Yuan, L.; Li, S.; Huo, D.; Zhou, W.; Wang, X.; Bai, D.; Hu, J. Studies on the Preparation and Photostability of Avobenzone and (2-Hydroxy)Propyl-β-Cyclodextrin Inclusion Complex. *J. Photochem. Photobiol., A* **2019**, *369*, 174−180.
(46) Lezcano, M.; Novo, M.; Al-Soufi, W.; Rodríguez-Núñez, E.; Tato, J. V. Complexation of Several Fungicides with β-Cyclodextrin: Determination of the Association Constants and Isolation of the Solid Complexes. *J. Agric. Food Chem.* **2003**, *51*, 5036−5040.
(47) Cruickshank, D. L.; Rougier, N. M.; Maurel, V. J.; De Rossi, R. H.; Buján, E. I.; Bourne, S. A.; Caira, M. R. Permethylated β-Cyclodextrin/Pesticide Complexes: X-Ray Structures and Thermogravimetric Assessment of Kinetic Parameters for Complex Dissociation. *J. Inclusion Phenom. Macrocyclic Chem.* **2013**, *75*, 47−56.
(48) Smith, V. J.; Rougier, N. M.; de Rossi, R. H.; Caira, M. R.; Buján, E. I.; Fernández, M. A.; Bourne, S. A. Investigation of the Inclusion of the Herbicide Metobromuron in Native Cyclodextrins by Powder X-Ray Diffraction and Isothermal Titration Calorimetry. *Carbohydr. Res.* **2009**, *344*, 2388−2393.
(49) Yáñez, C.; Cañete-Rosales, P.; Castillo, J. P.; Catalán, N.; Undabeytia, T.; Morillo, E. Cyclodextrin Inclusion Complex to Improve Physicochemical Properties of Herbicide Bentazon: Exploring Better Formulations. *PLoS One* **2012**, *7*, No. e41072.
(50) Cruickshank, D. L.; Bogdan, M.; Fărcas, S. I.; Bourne, S. A.; Caira, M. R. Investigation of the Inclusion of the Herbicide Cycluron in Native Cyclodextrins by X-Ray Diffraction, Nuclear Magnetic Resonance Spectroscopy and Isothermal Titration Calorimetry. *Supramol. Chem.* **2012**, *24*, 406−414.
(51) Balmas, V.; Delogu, G.; Sposito, S.; Rau, D.; Migheli, Q. Use of a Complexation of Tebuconazole with β-Cyclodextrin for Controlling Foot and Crown Rot of Durum Wheat Incited by Fusarium Culmorum. *J. Agric. Food Chem.* **2006**, *54*, 480−484.
(52) Yañez, C.; Araya, M.; Bollo, S. Complexation of Herbicide Bentazon with Native and Modified β-Cyclodextrin. *J. Inclusion Phenom. Macrocyclic Chem.* **2010**, *68*, 237−241.
(53) Yañez, C.; Günther, G. Is the Determination of the Association Constant of Cyclodextrin Inclusion Complexes Dependent on the Technique. *J. Chil. Chem. Soc.* **2014**, *59*, 2523−2525.
(54) Sheldrick, G. M. SHELXT - Integrated Space-Group and Crystal-Structure Determination. *Acta Crystallogr., Sect. A: Found. Adv.* **2015**, *71*, 3−8.
(55) Sheldrick, G. M. Crystal Structure Refinement with SHELXL. *Acta Crystallogr., Sect. C: Struct. Chem.* **2015**, *71*, 3−8.
(56) Dolomanov, O. V.; Bourhis, L. J.; Gildea, R. J.; Howard, J. A. K.; Puschmann, H. OLEX2: A Complete Structure Solution, Refinement and Analysis Program. *J. Appl. Crystallogr.* **2009**, *42*, 339−341.
(57) Spek, A. L. PLATON SQUEEZE: A Tool for the Calculation of the Disordered Solvent Contribution to the Calculated Structure Factors. *Acta Crystallogr., Sect. C: Struct. Chem.* **2015**, *71*, 9−18.
(58) Macrae, C. F.; Edgington, P. R.; McCabe, P.; Pidcock, E.; Shields, G. P.; Taylor, R.; Towler, M.; van de Streek, J. Mercury: Visualization and Analysis of Crystal Structures. *J. Appl. Crystallogr.* **2006**, *39*, 453−457.
(59) Degen, T.; Sadki, M.; Bron, E.; König, U.; Nénert, G. The HighScore Suite. *Powder Diffr.* **2014**, *29*, S13−S18.
(60) Boultif, A.; Louër, D. Powder Pattern Indexing with the Dichotomy Method. *J. Appl. Crystallogr.* **2004**, *37*, 724−731.
(61) Coelho, A. A. *TOPAS-Academic V4.1*; Coelho Software: Brisbane, Australia, 2007.
(62) Wadhwa, G.; Kumar, S.; Chhabra, L.; Mahant, S.; Rao, R. Essential Oil−Cyclodextrin Complexes: An Updated Review. *J. Incl. Phenom. Macrocycl. Chem.* **2017**, *89*, 39−58.
(63) Wang, Y.; Jiang, Z. T.; Li, R. Complexation and Molecular Microcapsules of Litsea Cubeba Essential Oil with β-Cyclodextrin and Its Derivatives. *Eur. Food Res. Technol.* **2009**, *228*, 865−873.
(64) Silva, A. F. R.; Monteiro, M.; Resende, D.; Braga, S. S.; Coimbra, M. A.; Silva, A. M. S.; Cardoso, S. M. Inclusion Complex of Resveratrol with γ-Cyclodextrin as a Functional Ingredient for Lemon Juices. *Foods* **2021**, *10*, 16.
(65) Jiang, Z.-T.; Tan, J.; Tan, J.; Li, R. Chemical Components and Molecular Microcapsules of Folium Artemisia Argyi Essential Oil with β-Cyclodextrin Derivatives. *J. Essent. Oil-Bear. Plants* **2016**, *19*, 1155−1169.
(66) Carrizosa, M. J.; Koskinen, W. C.; del Carmen Hermosín, M. Interactions of Acidic Herbicides Bentazon and Dicamba With Organoclays. *Soil Sci. Soc. Am. J.* **2004**, *68*, 1863−1866.
(67) Caira, M. R. On the Isostructurality of Cyclodextrin Inclusion Complexes and Its Practical Utility. *Rev. Roum. Chim.* **2001**, *46*, 371−386.
(68) Catenacci, L.; Sorrenti, M.; Bonferoni, M. C.; Hunt, L.; Caira, M. R. Inclusion of the Phytoalexin Trans-Resveratrol in Native Cyclodextrins: A Thermal, Spectroscopic, and X-Ray Structural Study. *Molecules* **2020**, *25*, No. 998.
(69) Ding, J.; Steiner, T.; Saenger, W. Structure of the γ-Cyclodextrin−1-Propanol−17H2O Inclusion Complex. *Acta Crystallogr., Sect. B: Struct. Sci., Cryst. Eng. Mater.* **1991**, *47*, 731−738.
(70) Trollope, L.; Cruickshank, D. L.; Noonan, T.; Bourne, S. A.; Sorrenti, M.; Catenacci, L.; Caira, M. R. Inclusion of Trans-Resveratrol in Methylated Cyclodextrins: Synthesis and Solid-State Structures. *Beilstein J. Org. Chem.* **2014**, *10*, 3136−3151.
(71) Rácz, C. P.; Borodi, G.; Pop, M. M.; Kacso, I.; Sánta, S.; Tomoaia-Cotisel, M. Structure of the Inclusion Complex of B-Cyclodextrin with Lipoic Acid from Laboratory Powder Diffraction Data. *Acta Crystallogr., Sect. B Struct. Sci.* **2012**, *68*, 164−170.
(72) Bethanis, K.; Tzamalis, P.; Tsorteki, F.; Kokkinou, A.; Christoforides, E.; Mentzafos, D. Structural Study of the Inclusion Compounds of Thymol, Carvacrol and Eugenol in β-Cyclodextrin by X-Ray Crystallography. *J. Inclusion Phenom. Macrocyclic Chem.* **2013**, *77*, 163−173.
(73) Kamitori, S.; Hirotsu, K.; Higuchi, T. Crystal and Molecular Structure of the γ-Cyclodextrin−12-Crown-4 1: 1 Inclusion Complex. *J. Chem. Soc. Chem. Commun.* **1986**, *9*, 690−691.

https://doi.org/10.1021/acssuschemeng.1c02749
ACS Sustainable Chem. Eng. 2021, 9, 12530−12539

(74) Paszko, T.; Matysiak, J.; Kamiński, D.; Pasieczna-Patkowska, S.; Huber, M.; Król, B. Adsorption of Bentazone in the Profiles of Mineral Soils with Low Organic Matter Content. *PLoS One* **2020**, *15*, No. e0242980.
(75) Bruzzoniti, M. C.; De Carlo, R. M.; Rivoira, L.; Del Bubba, M.; Pavani, M.; Riatti, M.; Onida, B. Adsorption of Bentazone Herbicide onto Mesoporous Silica: Application to Environmental Water Purification. *Environ. Sci. Pollut. Res.* **2016**, *23*, 5399−5409.
(76) Braga, D.; Grepioni, F.; Chelazzi, L.; Nanna, S.; Rubini, K.; Curzi, M.; Giaffreda, S. L.; Saxell, H. E.; Bratz, M.; Chiodo, T. Bentazon: Effect of Additives on the Crystallization of Pure and Mixed Polymorphic Forms of a Commercial Herbicide. *Cryst. Growth Des.* **2014**, *14*, 5729−5736.
(77) Food and Agriculture Organization of the United Nations. *FAO Specifications And Evaluations For Plant Protection Products - Bentazone*, 1999. p 4.
(78) BENTAZONE (sale sodico) . https://www.isprambiente.gov.it/contentfiles/00007800/7875-bentazon.pdf (accessed Mar 29, 2021).
(79) Tomlin, C. A World Compendium. The Pesticide Manual: Incorporating The Agrochemicals Handbook. *Br. Crop Prot. Counc.* **1996**, 1376.
(80) Kenaga, E. E. Predicted Bioconcentration Factors and Soil Sorption Coefficients of Pesticides and Other Chemicals. *Ecotoxicol. Environ. Saf.* **1980**, *4*, 26−38.
(81) EXTOXNET Extension Toxicology Network Pesticide Information Profiles. Bentazon. https://golsamco.com/doc/products/pdf/bentazonmsds.pdf (accessed Mar 29, 2021).

https://doi.org/10.1021/acssuschemeng.1c02749
ACS Sustainable Chem. Eng. 2021, 9, 12530−12539